

Electronic structure of $a\text{-Si}_{1-x}\text{N}_x\text{:H}$ and $a\text{-Ge}_{1-x}\text{N}_x\text{:H}$

S. S. Makler,* G. Martins da Rocha, and E. V. Anda†

*Instituto de Física, Universidade Federal Fluminense, Outeiro de São João Batista s/n, Niterói,
24 210 Rio de Janeiro, Brazil*

(Received 26 June 1989)

The electronic density of states of silicon nitrogen and germanium nitrogen alloys are calculated for the whole range of N concentrations. Also calculated are the local density of states at Si (Ge) atoms, at N atoms, and at sites with several configurations of dangling bonds. As single-site effective-medium theories are not applicable to semiconducting amorphous alloys due to the low values of the average coordination number ($3 \leq \langle z \rangle \leq 4$), we apply here a real-space renormalization formalism that produces accurate results with little computational effort. This formalism simultaneously includes diagonal and off-diagonal disorder, short-range order, and the charge-transfer effect. The results obtained here compare well with the experimental measurements.

I. INTRODUCTION

Semiconducting amorphous alloys are materials of increasing interest in recent years mainly due to their applications in microelectronics and solar-cell devices. Recently¹ samples of $a\text{-Ge}_{1-x}\text{N}_x$ have been grown for which an optimum gap size for solar-cell applications (approximately 1.6 eV) can be tailored, because its extremum values are about 1.1 eV for pure $a\text{-Ge:H}$ and 4.3 eV for stoichiometric $a\text{-Ge}_3\text{N}_4$. The alloy $a\text{-Si}_{1-x}\text{N}_x\text{:H}$ (Ref. 2) has been used as a dielectric in thin-film transistors² and it is also the basis of nonvolatile metal-nitride-oxide-semiconductor (MNOS) memory devices.³ Due to the fact that $a\text{-Si}_{1-x}\text{N}_x\text{:H}$ has a gap size E_g strongly dependent on nitrogen concentration^{4,5} it can be used as an optical window for solar cells⁶ and to prepare amorphous superlattices.^{6,7,8} $a\text{-Si}_{1-x}\text{C}_x\text{:H}$ (Ref. 9) and $a\text{-Si}_{1-x}\text{O}_x\text{:H}$ (Ref. 10) can also be used as optical windows, and $a\text{-Si}_{1-x}\text{Ge}_x\text{:H}$ has been studied experimentally¹¹ as a variable-band-gap material.

In order to understand the physical properties of these materials, it is necessary to study their electronic structures, and in particular the variations of the gap sizes with concentration and the existence of gap states due to dangling bonds, impurities, and other defects. These gap states can be traps for electrons or holes¹² and therefore they are important for the study of transport properties. They also control the doping properties of these materials. The Si dangling bond in silicon nitride can also be the memory trap in a MNOS device.¹³

The theoretical study of the electronic properties of semiconducting amorphous alloys is a hard task. These systems present both structural and chemical disorder. An idealized description of these materials is given by the continuous random network (CRN) (Ref. 14), which can be constructed by geometrical analogy¹⁵ or computer simulation.¹⁶ The calculations of the electronic properties of a CRN is highly expensive for actual computers.¹⁷ For amorphous alloys this network is characterized by a strong *structural* short-range order (SRO), a *chemical*

short-range disorder, and no long-range order. A real material can be thought of as a CRN with a distribution of defects: dangling bonds, vacancies, voids, impurities, etc.

Simplified disordered networks have been introduced in order to cope with the difficulties appearing in the CRN. The widely used Bethe lattice¹⁸ (or Cayley tree) can be easily treated (for chemically ordered materials) by transfer-matrix techniques.¹⁹ This pseudolattice is also useful as a boundary condition in clusters to study SRO properties of materials and defects in the so-called cluster-Bethe-lattice approximation²⁰ (CBL). Related structures such as Husimi cacti^{21,22} or gaskets^{23,24} were used as better approximations to the CRN.

The treatment of substitutional disorder is an old problem. Effective-medium theories were widely applied to study the electronic properties of metallic alloys. In order of increasing accuracy, they are the Nordheim-Mato virtual-crystal approximation (VCA), the Korringa average- t -matrix approximation (ATA), and the Seven-Taylor coherent-potential approximation (CPA).²⁵ The last one is a self-consistent procedure that gives the correct limits for both very low and very high concentrations. In spite of this fact it can be shown that the CPA is a zeroth-order theory in powers of $1/z$ (where z is the coordination number). It gives good agreement with numerical simulations for a fcc lattice ($z=12$), but it disagrees completely with "exact" histograms for one-dimensional random binary alloys (1D RBA) (Ref. 26) ($z=2$), and it yields very rough results for square and diamond lattices ($z=4$). This is due to the fact that the different chemical configurations of its neighbors produce very different local modes which cannot be averaged for low z . An alternative method to these single-site approximations consists of the exact treatment of small clusters as in the Bethe-Peierls approximation,^{27,28} leading to good results when self-consistency is applied to a boundary site.²⁶ However, even the molecular coherent-potential approximation (MCPA) is not capable of reproducing the *singularly continuous* spectrum²⁹ of a 1D RBA.

We will describe in this paper a method useful in treating the substitutional disorder even for low values of z . This method is based on a real-space renormalization procedure³⁰ applied to disordered chains by Gonçalves da Silva and Koiller³¹ (GK). The GK average procedure was widely discussed^{32–40} mainly within the context of 1D disordered systems. This procedure was extended to disordered Bethe lattices⁴¹ and Husimi cacti²² and was used to study the electronic properties of α -Si:H.^{34,42}



The paper is organized as follows. In Sec. II we present a self-consistent formalism to treat Bethe lattices. In Sec. III the extension of the simplest renormalized average method for a Hamiltonian with several orbitals per site is presented. In Sec. IV the limitations of that method are discussed and a new procedure is introduced to cope with them. The effects of short-range order and charge transfer are studied in the same section. Section V is devoted to show the procedures utilized to calculate local densities of states at atoms with dangling bonds and other defects. In Sec. VI the numerical procedures are briefly described. The results for α -Si_{1-x}N_x:H and α -Ge_{1-x}N_x:H are presented in Secs. VII and VIII, respectively. Finally, conclusions and comments are made in Sec. IX.

II. DECIMATION OF A DISORDERED BETHE LATTICE

The method will be illustrated here for the case of α -Si_{1-x}N_x:H, but it could be applied to a wide range of alloys.

Diffraction experiments^{43,44} show that bond-length and bond-angle distributions in α -Si₃N₄ (amorphous silicon nitride) are centered at the same position as in β -Si₃N₄, with a very small bond-length fluctuation. In this phase of crystalline silicon nitride, Si occupy slightly distorted tetrahedral sites and N are at planar or near-planar trigonal sites. The symmetry seems to be similar in α -Si₃N₄.¹² It has been shown that a nitrogen impurity in crystalline silicon is a deep donor with C_{3v} point-group symmetry.^{45,46}

The $8-n$ Mott rule establishes that N is threefold coordinated in an α -Si_{1-x}N_x:H for the whole range of concentrations $0 < x < \frac{4}{7}$.

Assuming this, we represent silicon and nitrogen by a fourfold-coordinated  and a threefold-coordinated  diagram, respectively. The connectivity of the lattice considered is illustrated in Fig. 1.

This lattice is a tree in the graph-theoretical sense that no loops or circuits (i.e., closed rings) are present in it.

The Hamiltonian describing the amorphous alloy is represented on a tight-binding basis with several orbitals per site:

$$\mathcal{H} = \sum_{\langle i,j \rangle, m, n} |im\rangle V_{ij}^{mn} |jn\rangle, \quad (1)$$

where i, j indicates the site and m, n the orbital.

Four orbitals are used for both nitrogen and silicon atoms. For Si they are the standard sp^3 orbitals, and for N they are three sp^2 coplanar orbitals and a perpendicular

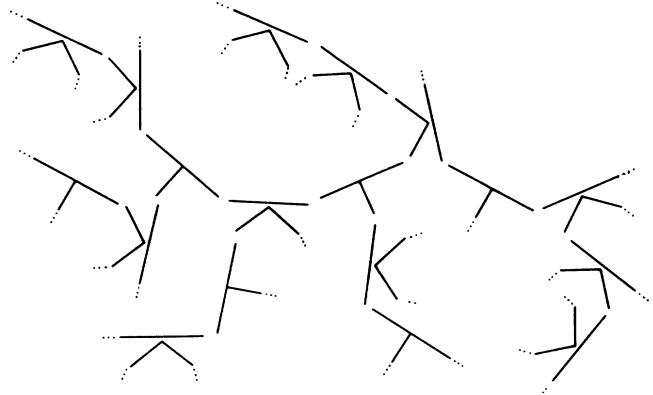


FIG. 1. A scheme of a Bethe lattice with a variable coordination number.

lar π orbital that participates in the bonds but in whose direction there is not a nearest neighbor.

Silicon-silicon and silicon-nitrogen bonds are illustrated in Figs. 2 and 3, respectively. The π orbital in Fig. 3 is represented by a point, indicating that its positive part is pointing outwards. In this model topological²² and quantitative⁴⁷ disorder are neglected. Therefore, dihedral angles are fixed. We adopt for the Si—Si bond the staggered configuration as in the crystalline case and for Si—N the configuration which is dominant in β -Si₃N₄ (i.e., orbitals i_1 and j_3 of Fig. 3 are in the same plane). There is strong evidence that nitrogen pairs are not present in the alloy.⁴⁸

The local energies of the isolated atoms and the hopping matrix elements between them are represented by 4×4 matrices.

$$\begin{aligned} \mathbb{E}_{\text{Si}} &= \begin{bmatrix} \epsilon & V_1 & V_1 & V_1 \\ V_1 & \epsilon & V_1 & V_1 \\ V_1 & V_1 & \epsilon & V_1 \\ V_1 & V_1 & V_1 & \epsilon \end{bmatrix} = \text{diag} \left(\begin{array}{c} \diagdown \\ \diagup \end{array} \right), \\ \mathbb{E}_{\text{N}} &= \begin{bmatrix} \epsilon_\pi & 0 & 0 & 0 \\ 0 & \epsilon_h & V_6 & V_6 \\ 0 & V_6 & \epsilon_h & V_6 \\ 0 & V_6 & V_6 & \epsilon_h \end{bmatrix} = \text{diag} \left(\begin{array}{c} \perp \\ \text{---} \end{array} \right), \\ \mathbb{V}_{\text{Si-Si}} &= \begin{bmatrix} V_5 & V_3 & V_4 & V_5 \\ V_5 & V_3 & V_5 & V_4 \\ V_4 & V_3 & V_5 & V_5 \\ V_3 & V_2 & V_3 & V_3 \end{bmatrix}, \\ \mathbb{V}_{\text{Si-N}} &= \begin{bmatrix} 0 & V_9 & V_{13} & V_{14} \\ -V_7 & V_9 & V_{10} & V_{11} \\ V_7 & V_9 & V_{10} & V_{11} \\ 0 & V_8 & V_{12} & V_{12} \end{bmatrix}. \end{aligned} \quad (2) \quad (3)$$

In order to illustrate the method, we consider first a Bethe lattice representing a fourfold-coordinated material without chemical disorder (a simplified model for an ideal α -Si) in which, as is shown in Fig. 4, the tree is arranged

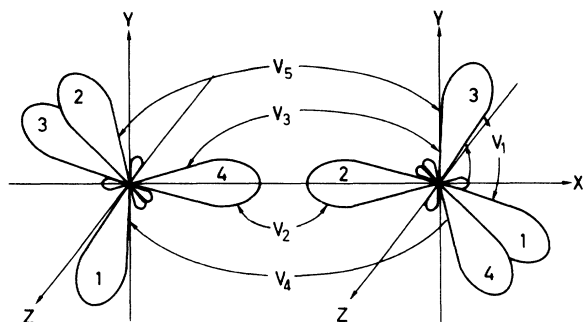


FIG. 2. The hopping matrix elements between two Si (or Ge) nearest neighbors.

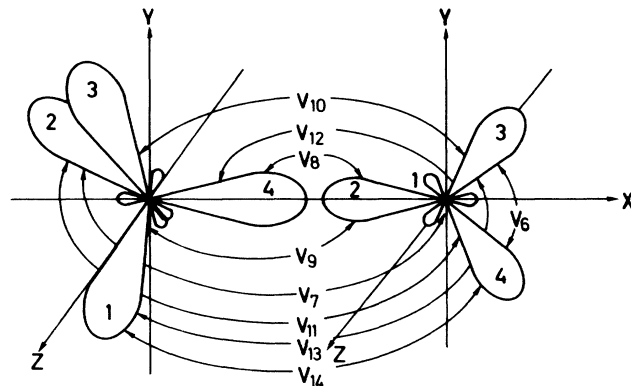


FIG. 3. The hopping matrix elements between a Si (or Ge) and a N atom.

as a linear chain of lattices. Each element of the linear chain of Fig. 4 can be represented diagrammatically as is shown in Fig. 5, where the arrows represent the self-energies associated with the network attached to the

bonds. We assume first that this network is not necessarily a piece of Bethe lattice, but is an arbitrary one. The self-energy of a chain constructed with these elements is

$$\begin{array}{c} \Sigma \\ \swarrow \searrow \\ \tilde{\Sigma} \end{array} = \dots \begin{array}{c} \Sigma \\ \swarrow \searrow \\ \tilde{\Sigma} \end{array} \begin{array}{c} \Sigma \\ \swarrow \searrow \\ \tilde{\Sigma} \end{array} \begin{array}{c} \Sigma \\ \swarrow \searrow \\ \tilde{\Sigma} \end{array} \begin{array}{c} \Sigma \\ \swarrow \searrow \\ \tilde{\Sigma} \end{array} \begin{array}{c} \Sigma \\ \swarrow \searrow \\ \tilde{\Sigma} \end{array} \begin{array}{c} \Sigma \\ \swarrow \searrow \\ \tilde{\Sigma} \end{array} \begin{array}{c} \Sigma \\ \swarrow \searrow \\ \tilde{\Sigma} \end{array} \begin{array}{c} \Sigma \\ \swarrow \searrow \\ \tilde{\Sigma} \end{array} \dots \quad (4)$$

It can be seen that only the Bethe lattice satisfies the fixed-point condition⁴¹

$$\tilde{\Sigma} = \Sigma \equiv \Sigma^* . \quad (5)$$

For a Bethe lattice with only one orbital per site this condition can be solved analytically.⁴¹ The result is the well known self-energy for an ordered Cayley tree,

$$\Sigma(\omega) = \frac{z}{2(z-1)} \{ (\omega - \epsilon) + [(\omega - \epsilon)^2 - 4(z-1)V^2]^{1/2} \} , \quad (6)$$

in which ϵ is the energy of the isolated atom, V the hopping element between nearest neighbors, and z the coordination number.

For a system with four orbitals per site, Eq. (4) has to be solved numerically. The standard transfer-matrix (TM) method also requires a numerical solution. The solution of Eq. (4) can be obtained as well by decimation, which re-

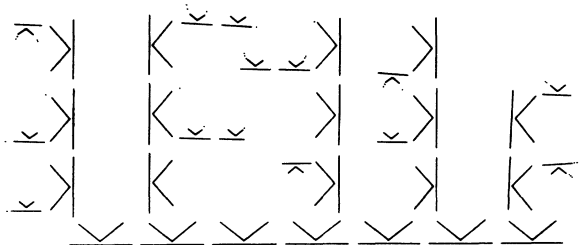


FIG. 4. A Bethe lattice represented as a linear chain of Bethe lattices.

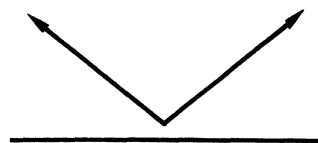


FIG. 5. A Si (or Ge) atom with two orbitals bonded to some lattice and two dangling bonds. This is the basic element of the linear chain used to solve the Bethe lattice.

quires far fewer iterations than the TM equation. This is due to the fact that decimation incorporates atoms at a geometrical rate, in contrast with the TM formalism, which does it arithmetically (the continued fraction).

Recently a diagonalization method to solve the ordered Bethe lattice with several orbitals per site was developed⁴² which is clearly faster than both decimation and TM methods. However, it will be probably very difficult to develop an extension of this diagonalization method for alloys.

In the case of $a\text{-Si}_{1-x}\text{N}_x(\text{Ge}_{1-x})$ we have two kinds of sites, namely, 1 for Si (Ge), 2 for N and two self-energy matrices. Equation (4) looks now as

$$\begin{array}{c} \Sigma_1 \\ \swarrow \quad \searrow \\ \tilde{\Sigma}_1 \leftarrow \tilde{\Sigma}_1 \end{array} = \dots \begin{array}{c} \Sigma_1 \quad \Sigma_2 \\ \swarrow \quad \uparrow \quad \searrow \quad \swarrow \quad \searrow \quad \uparrow \quad \swarrow \quad \Sigma_1 \\ \hline \uparrow \end{array}, \quad (7)$$

and we have a similar equation for N. Therefore we have self-energy matrices $\Sigma_1^\alpha, \Sigma_2^\beta$, where $\alpha=1,2,3,4$ and $\beta=2,3,4$ indicate the bond.

III. FIRST AVERAGE PROCEDURE

In order to quickly and accurately solve Eq. (7) we first adopt the GK average decimation procedure³¹⁻³⁵ extended to treat matrices. This approximation has proven to be much better than any of the known mean-field approximations, at least for low-coordinated systems, such as the case we are studying.

As we are working with 4×4 matrices, we take the simplest version of it for the sake of reducing the computer calculations. In order to derive the decimation recursive relations for an alloy with four orbitals per site, we label the basis orbitals:

$$\begin{array}{c} 1 \quad 3 \\ \swarrow \quad \searrow \\ 2 \quad 4 \end{array}, \quad \mathbb{E}_1 =$$

$$\begin{array}{c} 3 \\ | \\ 2 \quad 1 \quad 4 \end{array}, \quad \mathbb{E}_2 = \quad (8)$$

such that the chain defined in Eq. (4) follows always the sequence $\dots 2424 \dots$.

Its elements are

$$(1 - g_{\ell m}^{(k)} V_{\ell m}^{(k)} g_m^{(k)} V_{m \ell}^{(k)} - g_{\ell r}^{(k)} V_{\ell r}^{(k)} g_r^{(k)} V_{r \ell}^{(k)}) G_{\ell} - (g_{\ell m}^{(k)} V_{\ell m}^{(k)} g_m^{(k)} V_{m n}^{(k)}) G_h - (g_{\ell r}^{(k)} V_{\ell r}^{(k)} g_r^{(k)} V_{r s}^{(k)}) G_s = g_{\ell}^{(k)} \delta_{i0}, \quad (13)$$

where the indices n and s correspond to sites $i+2$ and $i-2$, respectively.

The renormalized virtual crystal method (RVCM) (Ref. 35) takes the average of this equation over the decimated degrees of freedom.

The remaining equations reproduce a new disordered system with its parameters renormalized. As the disordered is maintained at each step, this procedure takes into account chemical fluctuations at all orders.

We define matrices

$$M_{\ell m}^{(k)} \equiv 1 - g_{\ell m}^{(k)} V_{\ell m}^{(k)} g_m^{(k)} V_{m \ell}^{(k)} - g_{\ell r}^{(k)} V_{\ell r}^{(k)} g_r^{(k)} V_{r \ell}^{(k)}, \quad (14)$$

and make the decoupling

$$\begin{array}{c} \Sigma_1^{(0)} = \mathbb{E}_1 + \Sigma_1^1 + \Sigma_1^3 \\ = \begin{array}{c} \Sigma^1 \quad 2 \\ \swarrow \quad \searrow \\ 2 \quad 4 \end{array}, \end{array} \quad (9)$$

$$\begin{array}{c} \Sigma_2^{(0)} = \mathbb{E}_2 + \Sigma_2^3 \\ = \begin{array}{c} \Sigma^3 \\ | \\ 2 \quad 1 \quad 4 \end{array}, \end{array} \quad (10)$$

from which we can calculate the Green function

$$g_{\ell}^{(0)} = (\omega \mathbb{1} - \mathbb{H}_{\ell}^{(0)})^{-1}. \quad (11)$$

The self-energies are obtained from the equation of motion for the Green's functions which are solved using the decimation procedure

$$G_{\ell} - g_{\ell}^{(k)} V_{\ell m}^{(k)} G_m - g_{\ell}^{(k)} V_{\ell r}^{(k)} G_r = g_{\ell}^{(k)} \delta_{i0} \quad (12)$$

where subindices ℓ , m , and n correspond to sites i , $i+1$, and $i-1$, respectively, and can take the values 1 for Si and 2 for N. The index (k) labels the decimation step.

Now we use the equations corresponding to sites $i-1$ and $i+1$ to eliminate G_m and G_r , and we obtain

$$\begin{aligned} \langle M^{(k)} \rangle_{\ell} \langle G_{\ell} \rangle - \langle g_{\ell m}^{(k)} V_{\ell m}^{(k)} g_m^{(k)} V_{m n}^{(k)} \rangle \langle G_n \rangle \\ - \langle g_{\ell r}^{(k)} V_{\ell r}^{(k)} g_r^{(k)} V_{r s}^{(k)} \rangle \langle G_s \rangle = \langle g_{\ell}^{(k)} \rangle \delta_{i0}. \end{aligned} \quad (15)$$

Now we multiply by $(\langle M^{(k)} \rangle_{\ell})^{-1}$ to obtain an equation that will be isomorphous to the initial one, provided we define new g and V through the following recursion relations:

$$V_{\ell m}^{(k+1)} = \sum_{n=1}^2 P_{\ell n} (V_{\ell n}^{(k)} g_n^{(k)} V_{nm}^{(k)}), \quad (16)$$

which can be represented diagrammatically as

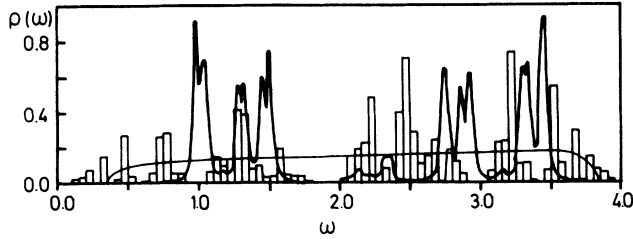


FIG. 6. The histogram represents the exact partially cumulated density of states (Ref. 61) PDCOS of an 1D RBA with one orbital per site (Ref. 27). The smooth curve is the approximated result obtained using CPA (Refs. 25 and 27). The curve with sharp peaks was obtained through the GK average procedure (Refs. 32 and 34).

$$\ell \xrightarrow{\quad} n = \ell \xrightarrow{\quad} m \xrightarrow{\quad} n \quad (17)$$

and

$$g_{\ell}^{(k+1)} = (\langle M^{(k)} \rangle_{\ell})^{-1} g_{\ell}^{(k)}. \quad (18)$$

This last relation is equivalent to the definition

$$\Sigma_{\ell}^{4(k+1)} = \Sigma_{\ell}^{4(k)} + \sum_{n=1}^2 P_{\ell n}^{(k)} (V_{\ell n}^{(k)} g_n^{(k)} V_{n \ell}^{(k)}), \quad (19)$$

with a diagrammatic representation given by

$$\Rightarrow_{\ell} = \Rightarrow_{\ell} + \begin{array}{c} \bullet \\ \diagup \quad \diagdown \\ \ell \quad \quad n \end{array} \quad (20)$$

In the diagrams above a point represents a site, a line represents a hopping transfer matrix V , and a double-line symbol represents a renormalized diagram. Here $P_{\ell n}$ is the probability of the first neighbor of ℓ being of n type.

In order to use Eqs. (16)–(20), $g_n^{(k)}$ is taken from Eq. (11), where

$$\mathbb{H}_{\ell}^{(k)} = \mathbb{H}_{\ell}^{(k)} + \Sigma_{\ell}^{4(k)} + \Sigma_{\ell}^{2(k)}, \quad (21)$$

and the initial values $H_{\ell}^{(0)}$ are given by Eq. (9) and $\Sigma^{(0)} = 0$.

When Eqs. (16) and (18) are iterated, the renormalized hopping diminishes, and for some k^* the condition

$$\sum_{i,j,\ell,m} |(V_{\ell m}^{(k^*)})_{ij}| < \varepsilon \quad (22)$$

is satisfied, and we obtain

$$\tilde{\Sigma}_{\ell}^{\alpha} \equiv \Sigma_{\ell}^{\alpha(k^*)}. \quad (23)$$

We can calculate now from Eq. (15) and $i = 0$

$$\langle G_{\ell} \rangle = g_{\ell}^{(k^*)}. \quad (24)$$

For the sake of comparison we show in Fig. 6 the density of states (DOS) for a one-dimensional random binary alloy (1D RBA) with one orbital per site.

IV. SECOND AVERAGE PROCEDURE

It can be seen from Eq. (12) that the GK procedure takes the average on the self-energy Σ . It is well known

that this kind of average produces, in the case of effective-medium theories, spurious densities of states in the gap.⁴⁹ The same problem appears in renormalization theories, as can be seen in Fig. 8.

In order to cope with this problem, a new renormalization formalism was proposed in a previous paper⁵⁰ which takes the average of the Green's function and produces better results even for an 1 RBA with only one orbital per site, as is shown in Fig. 7.

The formalism used here cannot be easily described in terms of renormalized g and V . It is better to rewrite Eq. (12) as

$$G_{\ell} - M_{\ell m}^{(k)} G_m - M_{\ell r}^{(k)} G_r = d_{\ell}^{(k)} \delta_{i0}, \quad (25)$$

where

$$M_{\ell m}^{(0)} = g_{\ell}^{(0)} V_{\ell m}^{(0)}, \quad d_{\ell}^{(0)} = g_{\ell}^{(0)}. \quad (26)$$

Now Eq. (13) is written as

$$L_{\ell mr}^{(k)} G_{\ell} - M_{\ell m}^{(k)} M_{mn}^{(k)} G_n - M_{\ell r}^{(k)} M_{rs}^{(k)} G_s = d_{\ell}^{(k)} \delta_{i0}, \quad (27)$$

where

$$L_{\ell mr}^{(k)} = 1 - M_{\ell m}^{(k)} M_{mr}^{(k)} - M_{\ell r}^{(k)} M_{rs}^{(k)}. \quad (28)$$

We first multiply Eq. (27) by $(L_{\ell mr}^{(k)})^{-1}$ and we take the average. The renormalized equation will be isomorphous to Eq. (25) if we define

$$M_{\ell n}^{(k+1)} = \langle (L_{\ell mr}^{(k)})^{-1} M_{\ell m}^{(k)} M_{mn}^{(k)} \rangle \quad (29)$$

and

$$d_{\ell}^{(k+1)} = \langle (L_{\ell mr}^{(k)})^{-1} d_{\ell}^{(k)} \rangle. \quad (30)$$

The formulae obtained now are as simple as in the first procedure, but we need to invert eight L matrices before averaging, in contrast with two for the GK method. We need further to invert matrices to get the Σ 's required to construct the Bethe lattice. This makes this second method computationally more expensive.

In order to construct the Bethe lattice we repeat this process beginning now with $\tilde{\Sigma}$ in the initial condition (9) until condition (5) is satisfied. All the steps in this process are very fast, except the inversion of the matrix required by Eq. (11).

To study semiconducting alloys as $a\text{-Si}_{1-x}\text{N}_x\text{:H}$, short-range order (SRO) and charge-transfer effects shall be included.

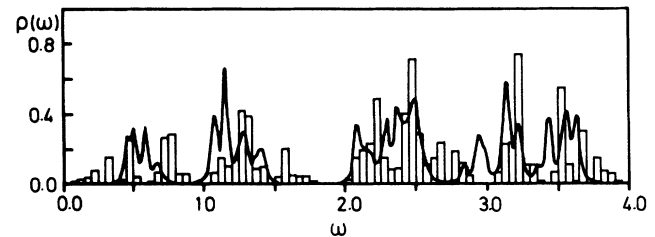


FIG. 7. The same as Fig. 6 but the curve with sharp peaks was obtained making the average on the Green function (Ref. 50).

It was pointed out at the beginning of this section that no nitrogen pairs are present in the alloy. This condition inhibits the possibility of having an alloy with concentration higher than $x = \frac{4}{7}$ (that corresponds to the stoichiometric compound $a\text{-Si}_3\text{N}_4\text{:H}$) if we neglect the presence of nitrogen hydrides.

The nitrogen concentration x' in the associated chain from which we constructed the Bethe lattice with variable coordination number is given by

$$x' = 3x / (4 - x) . \quad (31)$$

At the first decimation step, the conditional probability of having a silicon atom as the nearest neighbor of silicon is

$$P_{11}^{(0)} = (1 - 2x') / (1 - x') , \quad (32)$$

while the probability of silicon being a nearest neighbor of nitrogen is

$$P_{21}^{(0)} = 1 . \quad (33)$$

The first suffix refers to the atom at one site and the second to the atom at the neighbor site. Naturally

$$P_{/2}^{(k)} = 1 - P_{/1}^{(k)} . \quad (34)$$

However, after the first decimation step, this restriction does not hold any longer. The probability of having a renormalized silicon as a nearest neighbor of another renormalized silicon, $P_{11}^{(2)}$, is now the probability of these two silicon atoms to be second neighbors in the original chain. A simple probability calculation yields the result

$$P_{11}^{(1)} = P_{11}^{(0)} P_{11}^{(0)} + P_{12}^{(0)} P_{21}^{(0)} , \quad (35)$$

and for the $k + 1$ step of decimation

$$P_{ij}^{(k+1)} = P_{i1}^{(k)} P_{1j}^{(k)} + P_{i2}^{(k)} P_{2j}^{(k)} . \quad (36)$$

Therefore, the $P_{ij}^{(k)}$ matrix satisfies the relation

$$\mathbb{P}^{(k+1)} = (\mathbb{P}^{(k)})^2 , \quad (37)$$

that is equivalent to the scalar ones:

$$\begin{aligned} P_{21}^{(k+1)} &= P_{21}^{(k)} (D^{(k)} + 1) , \\ P_{11}^{(k+1)} &= P_{11}^{(k+1)} + D^{(k+1)} , \end{aligned} \quad (38)$$

where $D^{(k)}$ is the determinant of $P^{(k)}$ that obviously satisfies

$$D^{(k+1)} = (D^{(k)})^2 . \quad (39)$$

Relations (38) and (39) together with (34) and the initial conditions (32) and (33) properly take into account pair correlations for $a\text{-Si}_{1-x}\text{N}_x\text{:H}$ alloys.

The other important effect to be taken into account for the alloy is charge transfer. Nitrogen has an electron affinity greater than silicon. Therefore a nitrogen atom in a pure silicon matrix will get an electronic charge greater than 5 (corresponding to pure covalent bonding). The extra charge comes from the silicon atoms whose charge would be approximately 4 if they are surrounded only by silicon, or less depending on the number of nitrogen

atoms bonded to them. This charge transfer introduces a strong dependence upon local configuration of all nearest-neighbor matrix elements. For simplicity we considered this effect in an approximate way by taking the orbital energy ϵ as a function of concentration which is equivalent to a Hartree-Fock approximation for local electronic interaction. The charge transfer has been shown to be an essential ingredient to describe the experimental gap bowing for $a\text{-Si}_{1-x}\text{N}_x\text{:H}$.

V. DEFECTS IN AMORPHOUS ALLOYS

The knowledge of the self-energies Σ permits the calculation of the total electronic density of states (DOS) as well as the local densities of states (LDOS) at different defects and impurities present in the amorphous alloy.

Representing the self-consistent self-energies by a full arrow $\Sigma^* = \rightarrow$, the Green's functions can be calculated using Eq. (6) from the diagrams

$$\begin{aligned} H_{\text{Si}}^* &= \text{diagram 1} ; \\ H_{\text{N}}^* &= \text{diagram 2} . \end{aligned} \quad (40)$$

The imaginary part of the trace of the Green's-function matrices gives the LDOS at the silicon or nitrogen sites and their average the total DOS. A simple linear transformation from the silicon sp^3 and the nitrogen sp^2, p_π bases to the s, p_x, p_y, p_z ones gives a new representation for the Green's function from which the $s, p\sigma$, and p_π components of the spectrum can be obtained for both silicon and nitrogen.

The LDOS corresponding to one and two dangling bonds (DB) at Si or nitrogen sites are calculated from the diagrams

$$\begin{aligned} H_{\equiv\text{Si}} &= \text{diagram 3} , \\ H_{=\text{N}} &= \text{diagram 4} , \end{aligned} \quad (41)$$

$$\begin{aligned} H_{=\text{Si}} &= \text{diagram 5} , \\ H_{-\text{N}} &= \text{diagram 6} . \end{aligned} \quad (42)$$

Similarly, if we represent by a circle the self-energy due to an hydrogen atom (or F, Cl, etc.) $= -\circ$, the LDOS at a hydride configuration can be calculated from

$$\text{diagram 7} , \quad \text{diagram 8} , \quad (43)$$

$$\text{diagram 9} , \quad \text{diagram 10} . \quad (44)$$

The very interesting effect of doping impurities can

also be studied. Phosphorous in $a\text{-Si}_{1-x}\text{N}_x\text{:H}$ can be threefold (P_3) or fourfold (P_4) coordinated. The richest configuration is the first one. Using a dotted diagram for phosphorus, the LDOS at these impurity configurations can be obtained from

$$\begin{aligned} \mathbb{H}_{\text{P}_4} &= \begin{array}{c} \nearrow \text{---} \searrow \\ \text{---} \text{---} \text{---} \\ \nwarrow \text{---} \nearrow \end{array}, \\ \mathbb{H}_{\text{P}_3} &= \begin{array}{c} \text{---} \text{---} \text{---} \\ \text{---} \text{---} \text{---} \\ \uparrow \end{array}, \end{aligned} \quad (45)$$

in which the self-energy at the impurity atom Σ' can be easily related to the self-energies Σ . The LDOS for other impurities, such as B_3 , Ga_3 , As_3 , As_4 , etc. can be calculated in the same way. Results on hydrides and impurities will be published elsewhere.

VI. NUMERICAL PROCEDURE

The local density of states corresponding to the orbital ℓ at atom (or defect) i is calculated from the Green's-function matrix defined in (11):

$$\rho_{\ell i}(\omega) = -\frac{1}{\pi} \text{Im}[(g_{\ell})_{ii}]. \quad (46)$$

The calculation of the \mathbb{H}_{ℓ} corresponding to the six diagrams (40)–(42) can be carried out from the self-consistent solution of Eq. (5) $\Sigma^*(\omega)$, satisfied only by the Bethe lattice. This solution can be achieved iteratively in few steps if the starting point is sufficiently close to the solution. In each iteration step a random chain has to be solved, which can be done quickly and accurately by the decimation process described by Eqs. (16) and (18) or (29) and (30).

For a given concentration we start the calculation at an energy ω below the lowest band. For this energy $\Sigma(\omega) \cong 0$ and then $\mathbb{H}_{\ell} = \mathbb{E}_{\ell}$ is a good initial condition. This solution $\Sigma(\omega_0)$ is a better starting point for $\omega_1 = \omega_0 + \Delta\omega$ if $\Delta\omega$ is small. For $\omega_2 = \omega_1 + \Delta\omega$ we use as initial $\Sigma(\omega_2)$ the linearly extrapolated value obtained from $\Sigma(\omega_0)$ and $\Sigma(\omega_1)$, and for all the other energies we made quadratic extrapolations using the results obtained for the three previous points.

Unfortunately, the number of iterations required to obtain convergence increases rapidly near the band edges. In order to cope with this problem we perform Padé extrapolations for each element of Σ_{ℓ} matrices. Both normal and Padé sequences are calculated at each frequency. The iteration procedure is stopped when anyone of the

sequences reach convergence. About four iterations are needed inside the bands where the density of states is smooth. This number is reduced to one or two for points far outside the bands and augmented to about nine near the peaks. Finally, almost at the band edges up to twenty steps are necessary to get convergence of the Padé sequences, while more than 150 would be needed for the normal one. The convergence condition is defined by

$$\sum_{i,j,l} |(\Sigma_{\ell}^{(k)})_{ij} - (\Sigma_{\ell}^{(k-1)})_{ij}| < \epsilon_1. \quad (47)$$

We have taken $\epsilon_1 = 0.1$ eV, which warrants a precision of 10^{-3} in the densities of states. Within this accuracy, a value of $\Delta\omega = 0.05$ eV will be necessary. Lower values of $\Delta\omega$ makes the extrapolation process uneffective due to numerical noise. On the other hand, greater values for $\Delta\omega$ would not resolve the reach peak structure present in the LDOS.

VII. RESULTS FOR $a\text{-Si}_{1-x}\text{N}_x\text{:H}$

The parameters used in the calculation are shown in Table I. In the limit $x = 0$ (i.e., for pure $a\text{-Si:H}$) only ϵ and $V_1 - V_5$ are needed. They were taken from the work of Singh.⁵¹ The standard correction factor $4/\sqrt{12}$ was used to compensate the spurious band narrowing due to the finite surface size of the Bethe lattice. The values for $\epsilon_h, \epsilon_{\pi}$ and $V_6 - V_{14}$ were obtained from Robertson⁵² after transforming the s, p_x, p_y, p_z basis into the sp^3 (for Si) and the sp^2, p_{π} (for N). The energy of the sp^3 orbitals was taken to be a function of concentration $\epsilon(x) = -0.75 \text{ eV} + (0.43 \text{ eV})xP_{12}^{(0)}$ as was explained in Sec. IV.

In order to get numerical convergence near the band edges a small imaginary part η is added to the energy ω . This produces band tails, and the isolated modes outside the bands are transformed from δ functions to narrow Lorentzians of width η . A similar effect is present in actual systems due to quantitative disorder. Due to numerical considerations we have taken $\eta = 0.04$ eV. The finite value of η permits also the visualization of the relative strength of the gap modes in the LDOS.

In Figs. 8–14 we present the results obtained through the first procedure, where the average is taken on the self-energy Σ . The results for $x = 0$ and $x = \frac{4}{7}$ do not depend on the average, thus they coincide with those obtained by the second method and will be discussed there. For intermediate concentrations the results are less reliable, and in particular when the concentration changes from $x = 0.4$ to $x = 0.5$, it can be seen in Fig. 8 that a spurious density of states is moving from the valence band to the conduction band. As was discussed in Sec.

TABLE I. Tight-binding parameters for $a\text{-Si}_{1-x}\text{N}_x\text{:H}$ (in eV).

ϵ	ϵ_{π}	ϵ_h	V_1	V_2	V_3	V_4	V_5	V_6
-0.75	-3.00	-7.54	-1.90	-4.65	-0.23	0.95	-0.67	-5.25
V_7	V_8	V_9	V_{10}	V_{11}	V_{12}	V_{13}	V_{14}	
1.02	-7.33	-1.18	-0.20	0.66	0.73	1.11	-0.62	

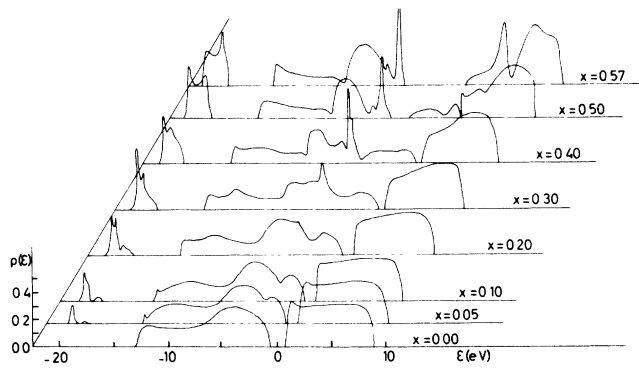


FIG. 8. The total DOS of $a\text{-Si}_{1-x}\text{N}_x\text{:H}$ calculated through the GK method (Refs. 31 and 33) (i.e., by taking the average on the self energies Σ). Note the spurious density of states traversing the gap for $0.4 < x < 0.5$.

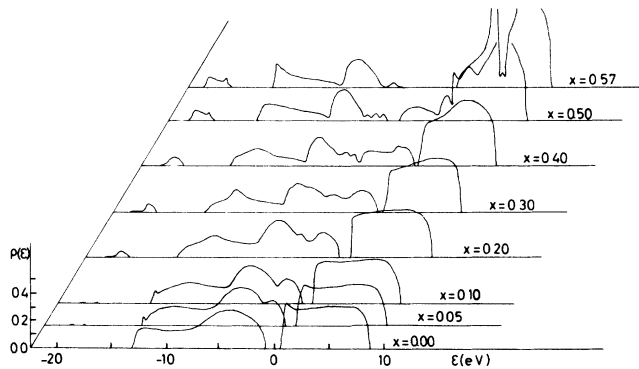


FIG. 9. The LDOS at a Si atom in the alloy.

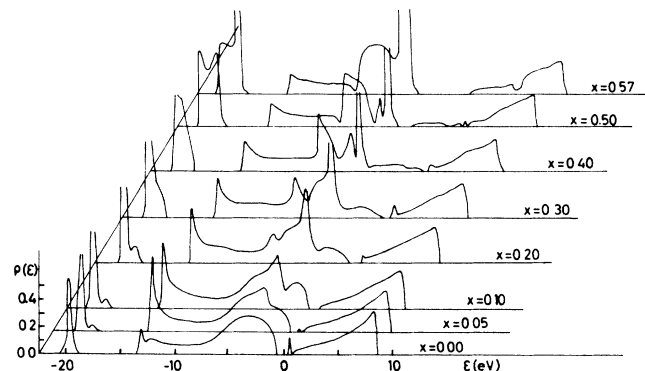


FIG. 10. The LDOS at a N atom.

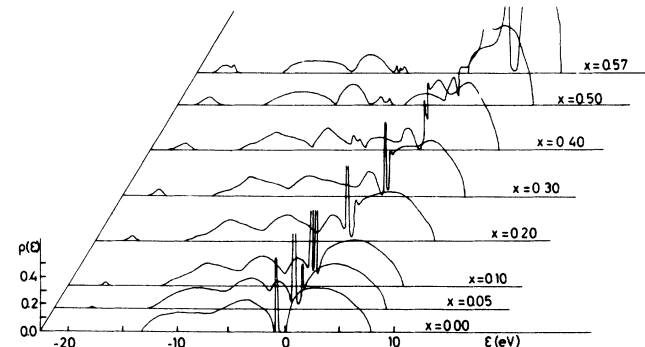


FIG. 11. The LDOS at a Si atom with a DB ($\equiv \text{Si}$).

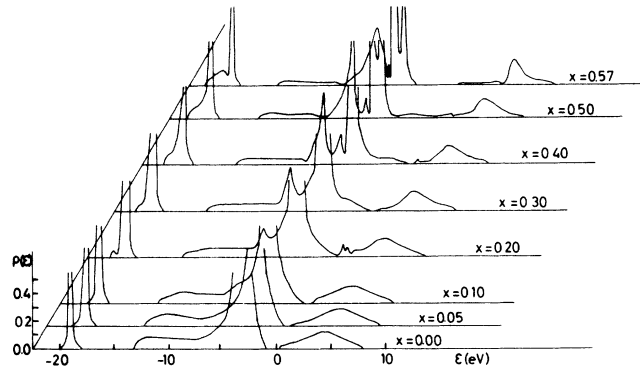


FIG. 12. The LDOS at a N atom with a DB ($\equiv \text{N}$).

IV, this is a characteristic of methods that take the average on Σ . It was pointed out in the same section that the results obtained by the second average procedure (i.e., by taking the average on the Green's function G) are better than the previous ones. Due to this fact we will restrict the discussion to Figs. 15–21, which present the results obtained through the best procedure.

In Fig. 15, $x=0$, is shown the DOS for pure $a\text{-Si:H}$ which presents the well-known characteristics of Bethe-lattice calculations of this system.^{34,53} The orbital energy ϵ was chosen in order to get the energies equal to zero at the center of the gap. The tops of valence and conduction bands are p type and the energy gap is $E_g = 1.6$ eV.

On the opposite side, for $x=0.57$, it shows the total density of states for stoichiometric $a\text{-Si}_3\text{N}_4\text{:H}$. The calculated value of the gap $E_g = 5.3$ eV coincides with the experimental results.⁴⁸ It can be seen that the top of the valence band is at the position of the p_π nitrogen level ($\epsilon_\pi = -3.00$ eV). Both valence and conduction bands present three peaks, as was obtained in Ref. 50, but we do not believe that our results for the conduction band are reliable because we have not taken into account the s^* orbital.^{54,55} The differences between our results and x-ray photoemission spectroscopy (XPS) measurements⁵⁶ are due to the large differences in the XPS matrix elements. This curve compares well also with the measurements obtained using synchrotron radiation⁴⁸ and qualitatively with the calculations of Ren and Ching.⁵⁷

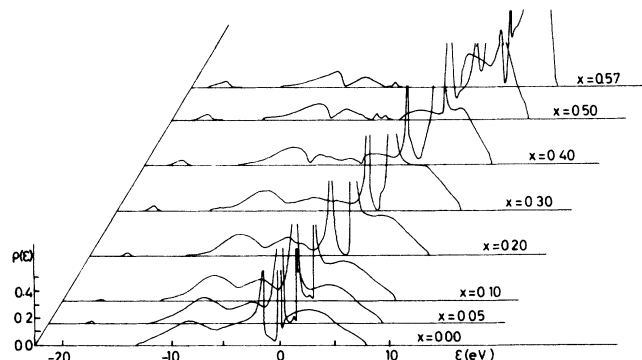


FIG. 13. The LDOS at a Si atom with two DB ($\equiv \text{Si}$).

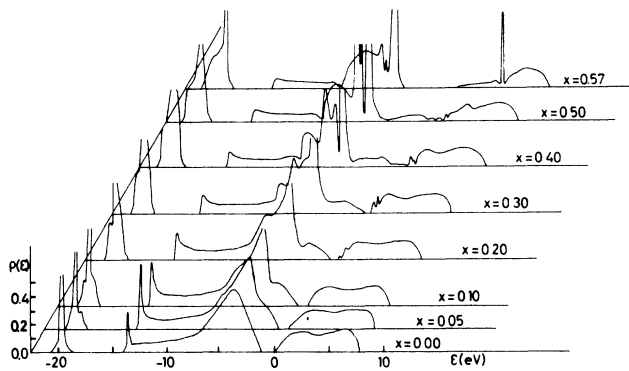


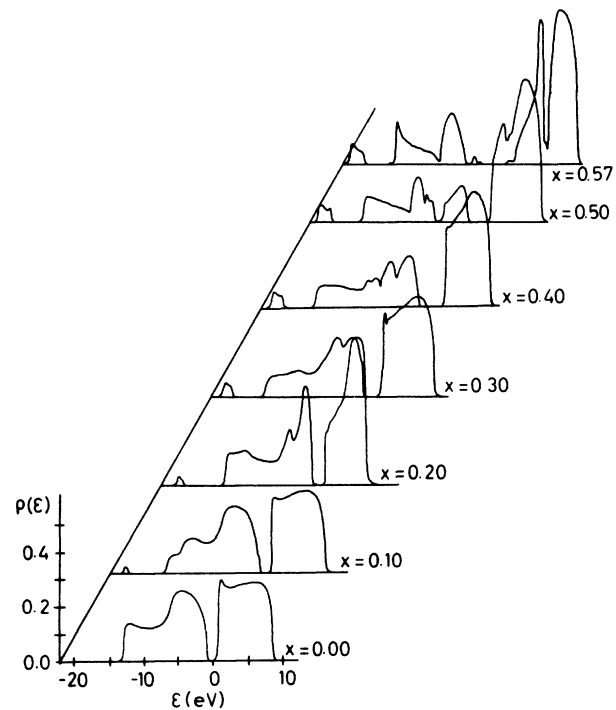
FIG. 14. The LDOS at a N atom with two DB (—N).

In the curve corresponding to $x = 0.1$ we can see a third band that arises up below the valence band (VB), due to the N s orbital placed at $\omega_s = -18.04$ eV. The position of this band remains almost fixed for all the concentration range and it coincides with the position of the strong peak observed by Kärcher *et al.*⁴⁸

For concentrations between $x = 0.2$ and $x = 0.4$ the development of the p_π peak and a slow broadening of the band gap are observed. The main transformation occurs for concentrations between 0.5 and 0.571.

In Fig. 16, $x = 0$, the LDOS at a Si atom coincides with the total DOS (Fig. 15, $x = 0$). This figure shows that the contributions of the N s and p_π levels are very small for all the range of concentrations. At high nitrogen concentrations the Si LDOS is big for the conduction band (CB) and small otherwise.

We show in Fig. 17 the LDOS of a nitrogen atom in

FIG. 16. The LDOS at a Si atom, obtained making $\langle G \rangle$.

the alloy. $x = 0$ corresponds to the LDOS of a N impurity in pure $a\text{-Si:H}$. The N s orbital bound to three Si sp^3 ones produces a localized mode at $\omega = -19.7$ eV. We can also see there two localized states corresponding to the bonding and antibonding modes with A_1 symmetry between the impurity and the lattice. The lowest (bond-

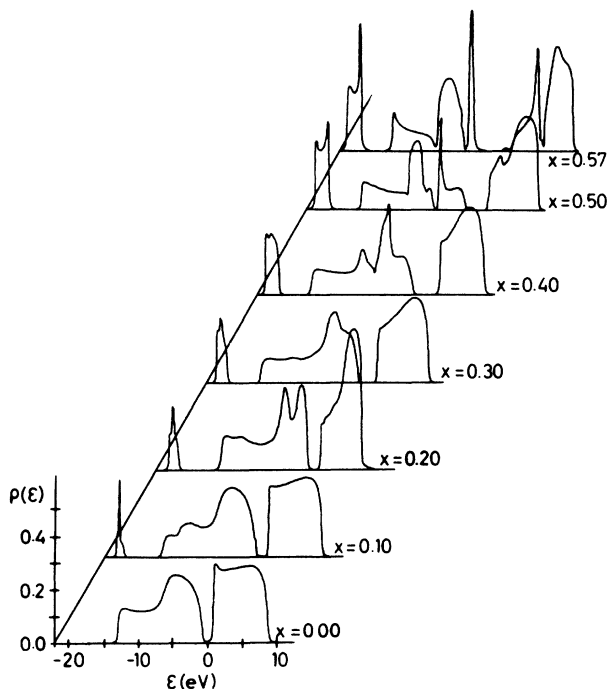
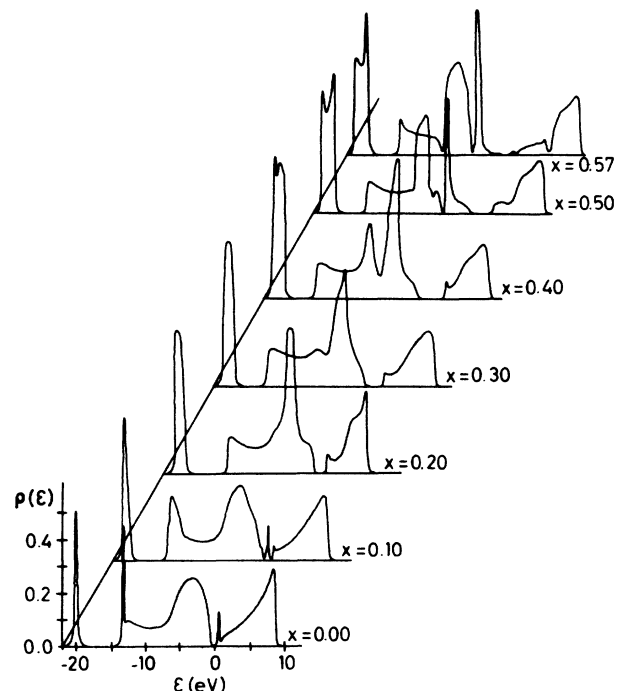
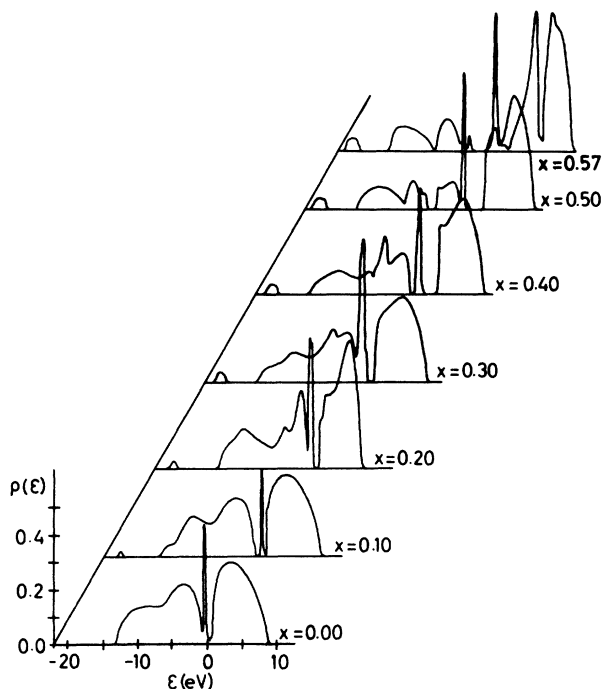
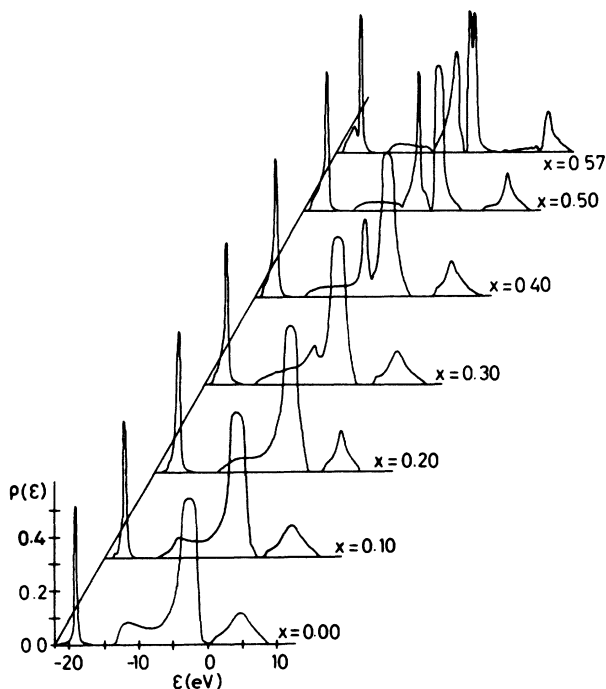
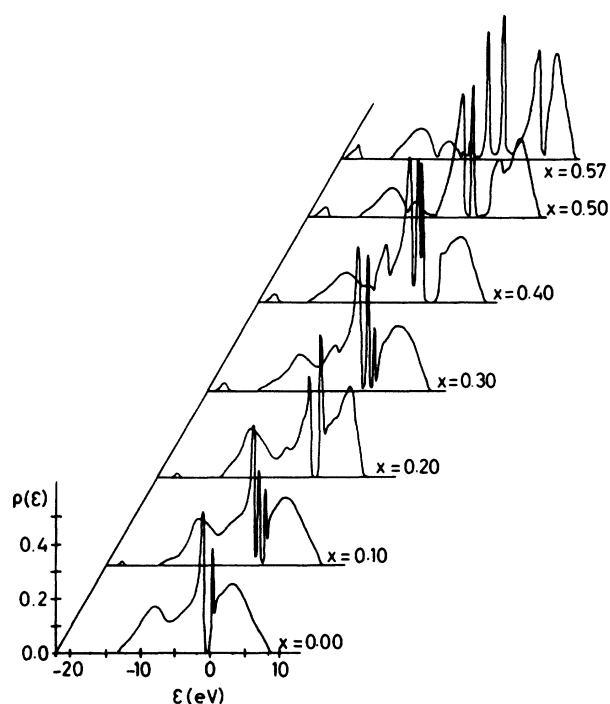
FIG. 15. The same as Fig. 8 but calculated by taking the average on the Green's functions G (Ref. 50).

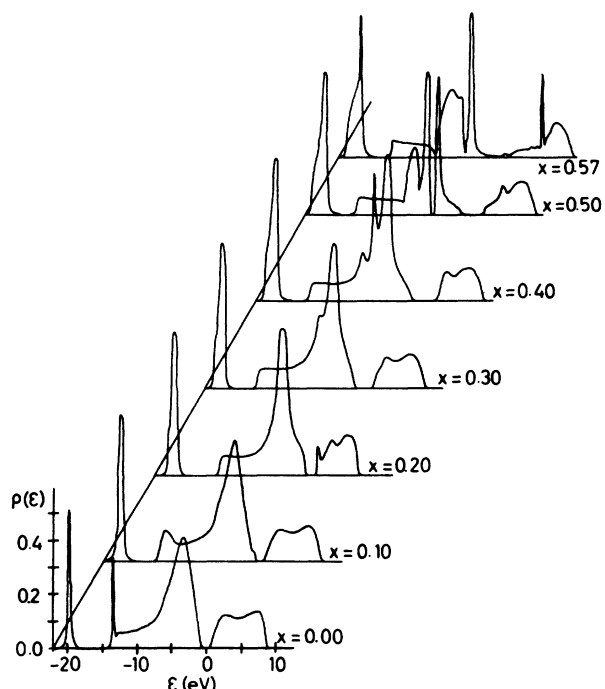
FIG. 17. The LDOS at a N atom.

FIG. 18. The LDOS at a Si atom with a DB (\equiv Si).

ing) state is located at $\omega = -12.4$ eV, whereas the highest (antibonding) one is inside the gap 0.45 eV below the bottom of the CB.⁵⁸ This last peak is at the same place where it was experimentally found by Brower,^{45,46} and that means that a nitrogen impurity is a deep donor. The small intensity of this gap mode at the nitrogen site is due

FIG. 19. The LDOS at a N atom with a DB (\equiv N).FIG. 20. The LDOS at a Si atom with two DB (\equiv Si).

to the fact that it is localized mainly on the first Si neighbors.⁵⁸ We can see also a strong resonance at the bottom of the VB. For concentrations greater than $x = 0.2$ the A_1 peaks disappear and the p_π peak develops. For $x > 0.3$ a second peak develops at the VB. The contribution of the N LDOS to the lowest and valence band is

FIG. 21. The LDOS at a N atom with two DB (\equiv N).

big, and it is very small at the beginning of the CB.

In Fig. 18, $x=0$, we can see in the gap 0.43 eV above the top of the valence band the well-known strongly localized state of a Si dangling bond (DB). This peak remains contaminating the gap for the whole range of concentrations.

Figure 19 shows the LDOS at a N atom with a dangling bond. The curve $x=0$ shows that such an impurity in pure Si has its lowest localized state shifted to $\omega = -19.05$ eV. There is an enhancement of the density of states near the p_π level. As in the case of a N impurity, we can see also the resonance at the bottom of the VB, but no gap states are localized at this defect.

We can see in Fig. 20 the results for the LDOS at a Si atom with two DB's. The interaction V_1 splits the gap state in two modes. The lowest mode merges slightly (0.2 eV) into the VB and the highest one enters the CB (0.3 eV, approximately). It can be seen that this defect also contaminates the gap for the whole range of concentrations.

At a N impurity with two DB's in pure $a\text{-Si:H}$ —Fig. 21, $x=0$ —the lowest mode is shifted to $\omega = -18.65$ eV, and the peak near the p_π level becomes stronger. This impurity does not produce states in the gap.

VII. RESULTS FOR $a\text{-Ge}_{1-x}\text{N}_x\text{:H}$

The tight-binding parameters for Ge-Ge were obtained from the work of Harrison,⁵⁴ whereas those corresponding to Ge-N were obtained by scaling the Si-N ones (described in the preceding section) following the d^{-2} law.⁵⁹ These parameters are shown in Table II. As in the case of $a\text{-Si}_{1-x}\text{N}_x\text{:H}$ it is supposed that the role of hydrogen in the material is essentially to terminate the dangling

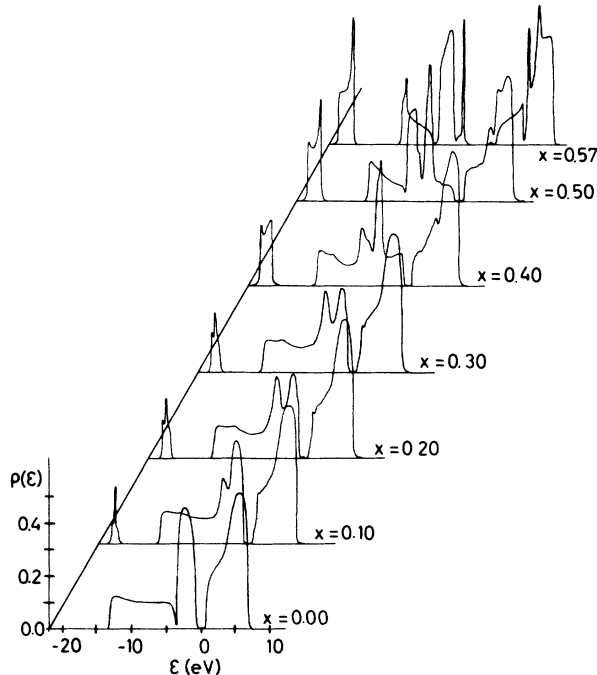


FIG. 22. The total DOS of $a\text{-Ge}_{1-x}\text{N}_x\text{:H}$ calculated also by the second average procedure ($\langle G \rangle$).

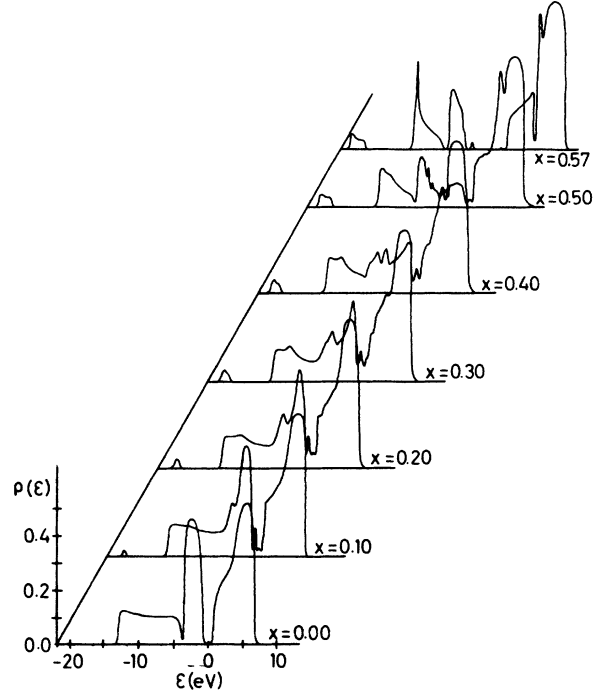


FIG. 23. The LDOS at a Ge atom.

bonds (mainly N).⁶⁰

Figure 22 shows the DOS of $a\text{-Ge}_{1-x}\text{N}_x\text{:H}$. For $x=0$ corresponding to pure $a\text{-Ge:H}$, the gap obtained is $E_g = 1.1$ eV in agreement with the experimental results.⁶⁰ The centers of the valence and conduction bands are less

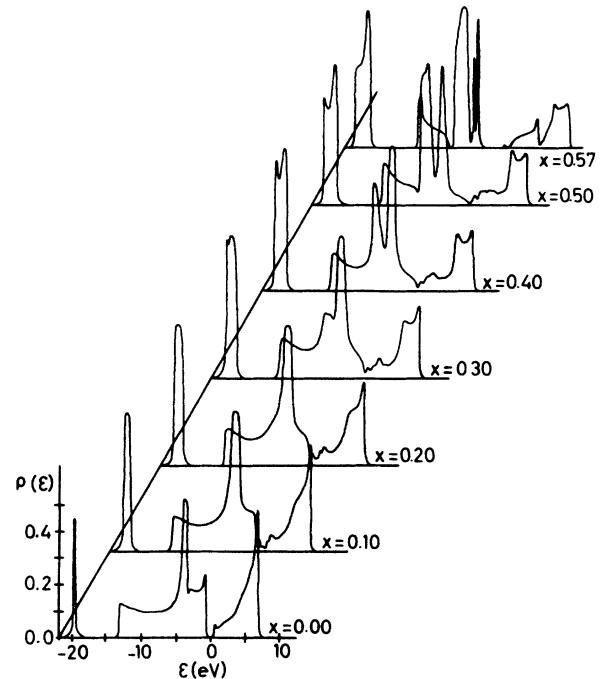
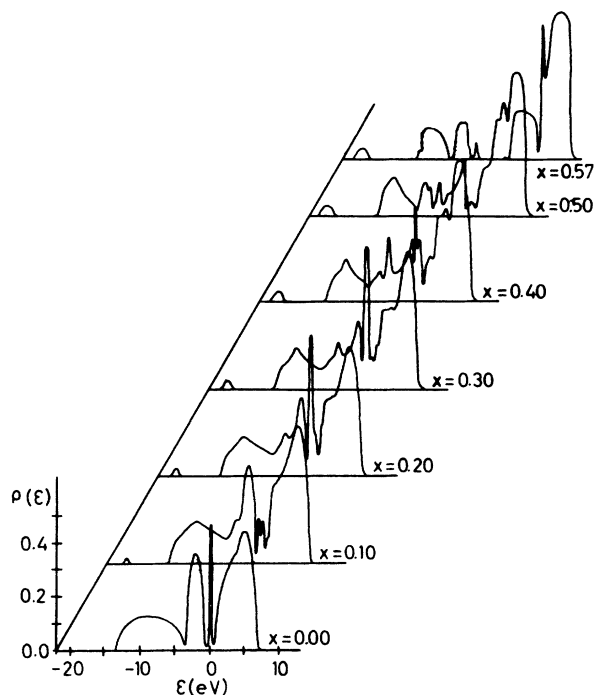
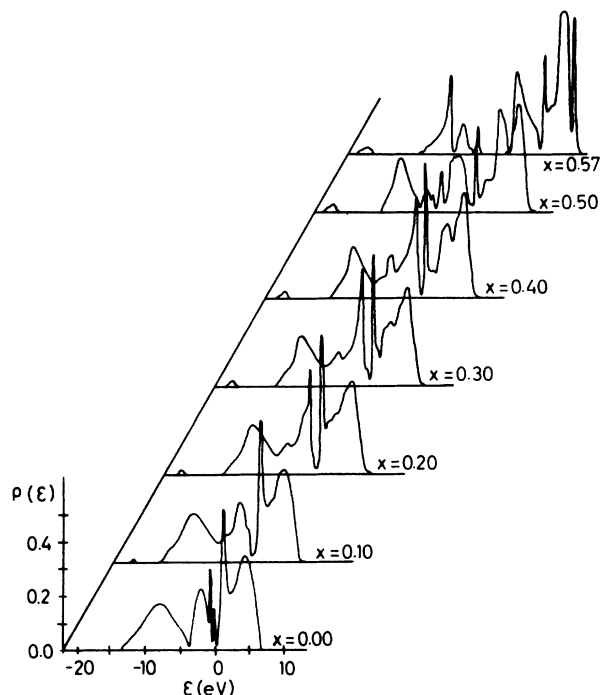


FIG. 24. The LDOS at a N atom.

FIG. 25. The LDOS at a Ge atom with a DB (\equiv Ge).

separated than in the case of α -Si:H, because the separation is determined by V_2 . For increasing concentrations we can observe the development of the N s and p_π peaks. The gap remains unaltered up to $x \approx 0.5$ and after that it grows quickly to reach the value $E_g = 4.7$ for $x = \frac{4}{7}$.

The electronic structure of stoichiometric

FIG. 27. The LDOS at a Ge atom with two DB (\equiv Ge).

α -Ge₃N₄:H—Fig. 22, $x = 0.57$ —is similar to that of α -Si₃N₄:H except for an additional peak in the middle of the conduction band. The top of the valence band is a lone pair N p_π peak.

In a first global calculation we found the gap contaminated by numerical noise, which was further eliminated

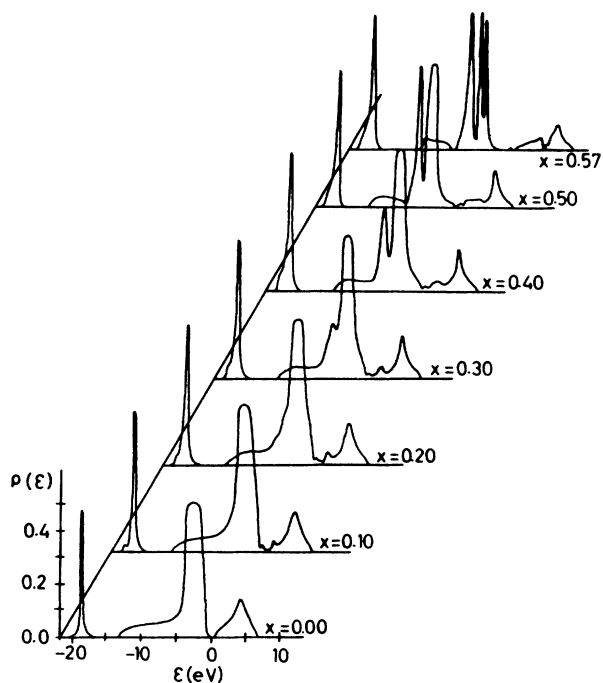
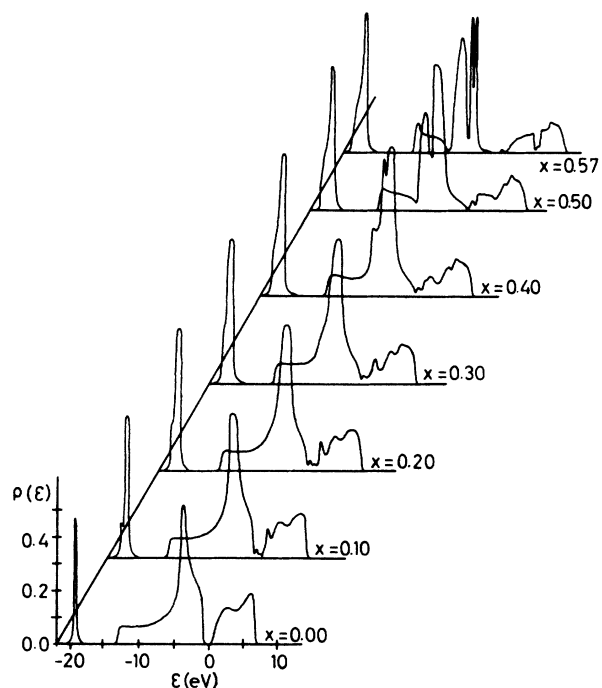
FIG. 26. The LDOS at a N atom with a DB (\equiv N).FIG. 28. The LDOS at a N atom with two DB (\equiv N).

TABLE II. Tight-binding parameters for $a\text{-Ge}_{1-x}\text{N}_x\text{:H}$ (in eV).

ϵ	ϵ_π	ϵ_h	V_1	V_2	V_3	V_4	V_5	V_6
-0.75	-3.00	-7.54	-2.15	-4.03	-0.27	0.39	-0.39	-5.25
V_7	V_8	V_9	V_{10}	V_{11}	V_{12}	V_{13}	V_{14}	
0.81	-5.84	-0.91	-0.14	0.51	0.56	0.85	-0.48	

in a more detailed (and slow) calculation for this region.

We present in Fig. 23 the average LDOS at a Ge atom for several N concentrations. The qualitative aspects of these curves are very close to those of $a\text{-Si}_{1-x}\text{N}_x\text{:H}$ described in the last section.

In Fig. 24 the LDOS's at a N atom in the alloy are shown. The A_1 bonding and antibonding levels merge into the valence and conduction bands, respectively. For pure $a\text{-Ge:H}$ the distance between the antibonding level and the bottom of the conduction band is too small to confirm whether a N impurity is a donor or not because this situation may be modified by small changes in the tight-binding parameters.

The LDOS at a Ge atom with a DB for pure Ge (Fig. 25, $x=0$) shows the characteristic peak at the center of the gap, but it disappears for N concentrations higher than $x=0.4$.

We can see that the qualitative behavior of a N atom with a DB in $a\text{-Ge}_{1-x}\text{N}_x\text{:H}$ (Fig. 26) is the same as in $a\text{-Si}_{1-x}\text{N}_x\text{:H}$ (Fig. 19).

A Ge atom with two DB's does not produce states in the gap for stoichiometric $a\text{-Ge}_3\text{N}_4\text{:H}$ (Fig. 27, for $x=0.57$), as is the case of silicon nitride (Fig. 20, $x=0.57$).

Figure 28 shows the LDOS at a N atom with two DB's. By contrast, with the case of Si (Fig. 21) it can be seen that for pure Ge the A_1 bonding state does not appear as an isolated mode. The same occurs with the peak at the center of the conduction band for the stoichiometric compound.

IX. CONCLUSIONS

The accuracy of calculations of the electronic properties of semiconducting amorphous alloys is limited, in most cases, by the treatment of disorder. The standard

single-site effective-medium approximations (like the CPA) are not reliable when the coordination number is small. On the other hand, the recursion method yields better results than the CPA, but is computationally slow. The real-space renormalization method used in our calculation incorporates in a natural way diagonal and off-diagonal disorder, short-range order, and charge-transfer effects, and is at least as good as the recursion method, and it is much faster.

The shortcomings of our calculation come mainly from the choice of the tight-binding parameters, the use of the Bethe lattice, and the treatment of the electronic repulsion, the average procedure being a minor limitation.

The results obtained for pure Si (Ge) and for stoichiometric nitrides compare well with the experimental measurements. For intermediate concentrations, the calculated band structure of $a\text{-Si}_{1-x}\text{N}_x\text{:H}$ agrees with the measurements of Kärcher *et al.*⁴⁸ as was discussed above.

As we have not considered explicitly the excited (or the s^*) orbitals, our results for the conduction band are not accurate.

To the best of our knowledge, for the case of $a\text{-Ge}_{1-x}\text{N}_x\text{:H}$ no experimental data are available to compare with our theoretical results. Our calculations for $a\text{-Ge}_{1-x}\text{N}_x\text{:H}$ show no major qualitative differences with respect to $a\text{-Si}_{1-x}\text{N}_x\text{:H}$, besides the fact that the energy gap is smaller for low nitrogen concentrations. This property could be very useful for solar-cell applications of this alloy.

ACKNOWLEDGMENTS

This work was partially financed by Conselho Nacional de Desenvolvimento Científico e Tecnológico (CNPq) and Financiadora de Estudos e Projetos (FINEP), Brazil.

*Present address: Institut de Physique, Université de Liège, Bâtiment B5, B-4000 Sart Tilman (Liège), Liège 1, Belgium.

†Present address: Departamento de Física de la Materia Condensada, Universidad Autónoma de Madrid, E-28049 Madrid, Spain.

¹I. Chambouleyron, Appl. Phys. Lett. **47**, 117 (1985); I. Chambouleyron, F. Marques, J. Cisneros, F. Alvarez, S. Mohlecke, W. Losch, and I. Pereyra, J. Non-Cryst. Solids **77/78**, 1309 (1985).

²E. Bustarret, M. Bensouda, M. C. Habrard, J. C. Bruyère, S. Poulin, and S. C. Gujrathi, Phys. Rev. B **38**, 8171 (1988); M. J. Powell, Appl. Phys. Lett. **43**, 597 (1983).

³P. Bulk, in *Insulating Films on Semiconductors*, edited by J. F.

Vewey and D. R. Wolters (North-Holland, Amsterdam, 1983), p. 204.

⁴I. Chambouleyron, F. Alvarez, C. Constantino, and J. I. Cisneros, in *Proceedings of the 5th E.C. Photovoltaic Solar Energy Conference* (Reidel, Dordrecht, 1983), p. 818.

⁵F. Alvarez, I. Chambouleyron, C. Constantino, and J. I. Cisneros, Appl. Phys. Lett. **44**, 116 (1984); I. Chambouleyron, F. Alvarez, L. R. Tessler (unpublished).

⁶N. Ibraki and H. Fritzsche, Phys. Rev. B **30**, 5791 (1984).

⁷B. Abeles and T. Tiedje, Phys. Rev. Lett. **51**, 2003 (1983).

⁸M. Hirose and S. Miyazaki, J. Non-Cryst. Solids **66**, 327 (1984).

⁹S. Liedtke, K. Jahn, F. Finger, and W. Fuhs, J. Non-Cryst. Solids **97/98**, 1083 (1987); A. Cattalano, R. V. D. Aiello, J.

- Dresner, B. Faugham, A. Firestes, J. Kane, H. Schade, Z. E. Smith, G. Schwartz, and A. Friane (unpublished).
- ¹⁰J. C. Knights, R. A. Street and G. Lucovsky, *J. Non-Cryst. Solids* **35/36**, 279 (1980).
- ¹¹J. Riestein, F. Finger, W. Fuhs, and S. Liedtke, *Solid State Commun.* **67**, 211 (1988); B. Von Roeden, D. K. Paul, J. Blake, R. W. Collins, G. Moddel, and W. Paul, *Phys. Rev. B* **25**, 7678 (1982); F. Finger, W. Fuhs, G. Beck, and R. Carius, *J. Non-Cryst. Solids* **97/98**, 1015 (1987); R. Carius, F. Finger, and W. Fuhs, *J. Non-Cryst. Solids* **97/98**, 1067 (1987); F. Finger, W. Fuhs, and R. Carius, *Philos. Mag. Lett.* **57**, 235 (1987); W. Fuhs, *Phys. Scr.* **T25**, 268 (1989).
- ¹²J. Robertson, *J. Appl. Phys.* **54**, 4490 (1983).
- ¹³J. Robertson and M. J. Powell, *Appl. Phys. Lett.* **44**, 415 (1984).
- ¹⁴W. H. Zaccariassen, *J. Am. Chem. Soc.* **54**, 3841 (1932).
- ¹⁵D. E. Polk, *J. Non-Cryst. Solids* **5**, 365 (1971).
- ¹⁶D. Henderson and F. Herman, *J. Non-Cryst. Solids* **8**, 359 (1972).
- ¹⁷W. Y. Ching, D. J. Lam, and C. C. Lin, *Phys. Rev. Lett.* **42**, 805 (1979).
- ¹⁸C. Domb, *Adv. Phys.* **9**, 149 (1960).
- ¹⁹M. F. Thorpe, in *Excitations in Disordered Systems*, edited by M. F. Thorpe (Plenum, New York, 1981), p. 85.
- ²⁰L. Martín-Moreno, E. Martínez, J. A. Vergés, and F. Yndurain, *Phys. Rev. B* **35**, 9683 (1987); E. Louis and J. A. Vergés, *Solid State Commun.* **60**, 157 (1987); G. Gómez-Santos, and J. A. Vergés, *J. Phys. C* **20**, 5501 (1987); J. D. Joannopoulos and M. L. Cohen, *Solid State Physics* **31**, 71 (1976); L. Martín-Moreno and J. A. Vergés, *J. Phys. C* **19**, 6751 (1986).
- ²¹M. F. Thorpe, D. Weaire, and R. Alben, *Phys. Rev. B* **7**, 3777 (1973).
- ²²E. V. Anda, S. S. Makler, M. A. Continentino, and P. M. de Oliveira, *J. Phys. C* **17**, 4101 (1984).
- ²³A. Latgé, S. S. Makler, and E. V. Anda, *Phys. Status Solidi B* **141**, 163 (1987).
- ²⁴F. Domany, S. Alexander, D. Bensimon, and L. Kadanoff, *Phys. Rev. B* **28**, 3110 (1983).
- ²⁵A. D. Zdetsis, E. N. Economou, D. A. Papaconstantopoulos, and N. Flytzanis, *Phys. Rev. B* **31**, 2410 (1985); W. E. Pickett, D. A. Papaconstantopoulos, and E. N. Economou, *Phys. Rev. B* **28**, 2232 (1983); R. Elliot, J. Krumhansl, and P. Leath, *Rev. Mod. Phys.* **46**, 465 (1974); A. D. Zdetsis (unpublished).
- ²⁶W. H. Butler, *Phys. Rev. B* **10**, 4499 (1973).
- ²⁷H. A. Bethe, *Proc. R. Soc. London, Ser. A* **150**, 552 (1935).
- ²⁸F. Brouers, M. Cyrot, and F. Cyrot-Lackman, *Phys. Rev. B* **7**, 4370 (1973).
- ²⁹K. Ishii, *Prog. Theor. Phys. (Suppl.)* **53**, 77 (1973).
- ³⁰H. Aoki, *Solid State Commun.* **31**, 999 (1979).
- ³¹C. E. T. Gonçalves da Silva and B. Koiller, *Solid State Commun.* **40**, 215 (1981).
- ³²J. M. Langlois, A.-M. S. Tremblay, and B. W. Southern, *Phys. Rev. B* **28**, 218 (1983).
- ³³B. Koiller, M. O. Robbins, M. A. Davidovich, and C. E. T. Gonçalves da Silva, *Solid State Commun.* **45**, 955 (1983).
- ³⁴E. V. Anda and S. S. Makler, in *Proceedings of the 17th International Conference on the Physics of Semiconductors, San Francisco*, edited by J. D. Chadi and W. A. Harrison (Springer-Verlag, New York, 1985), p. 783.
- ³⁵M. O. Robbins and B. Koiller, *Phys. Rev. B* **27**, 7703 (1983).
- ³⁶D. A. Lavis, B. W. Southern, and S. G. Davidson, *J. Phys. C* **18**, 1387 (1985).
- ³⁷G. Albinet and A.-M. S. Tremblay, *Phys. Rev. B* **28**, 232 (1983).
- ³⁸B. W. Southern, A. A. Kumar, and J. A. Asharaff, *Phys. Rev. B* **28**, 1785 (1985).
- ³⁹B. W. Southern, A. A. Kumar, P. D. Loly, and A.-M. S. Tremblay, *Phys. Rev. B* **27**, 405 (1983).
- ⁴⁰J. José, *J. Phys. A* **16**, L205 (1983).
- ⁴¹J. d'Albuquerque e Castro, *J. Phys. C* **17**, 5945 (1984).
- ⁴²J. Urias and L. Falicov, *Phys. Rev. B* **30**, 6931 (1984).
- ⁴³T. Aiyama, T. Fukunaga, K. Niihara, T. Hirai, and K. Suzuki, *J. Non-Cryst. Solids* **33**, 131 (1979).
- ⁴⁴M. Misawa, T. Fukunaga, K. Niihara, T. Hirai, and K. Suzuki, *J. Non-Cryst. Solids* **34**, 313 (1979).
- ⁴⁵K. L. Brower, *Phys. Rev. Lett.* **44**, 1627 (1980).
- ⁴⁶K. L. Brower, *Phys. Rev. B* **26**, 6040 (1982).
- ⁴⁷N. V. Cohan and M. Weissmann, *Solid State Commun.* **16**, 853 (1975).
- ⁴⁸R. Kärcher, L. Ley, and R. L. Johnson, *Phys. Rev. B* **30**, 1896 (1984).
- ⁴⁹R. Kittler and L. M. Falicov, *J. Phys. C* **9**, 4259 (1976).
- ⁵⁰A. Latgé and E. V. Anda, *J. Phys. C* **21**, 4251 (1988).
- ⁵¹J. Singh, *Phys. Rev. B* **23**, 4156 (1981).
- ⁵²J. Robertson, *Philos. Mag. B* **44**, 215 (1981).
- ⁵³D. C. Allan, J. D. Joannopoulos, and W. B. Pollard, *Phys. Rev. B* **25**, 1065 (1982).
- ⁵⁴W. A. Harrison, *Phys. Rev. B* **27**, 3592 (1983).
- ⁵⁵S. Louie, *Phys. Rev. B* **22**, 1933 (1980).
- ⁵⁶Z. A. Weinberg and R. A. Pollak, *Appl. Phys. Lett.* **27**, 254 (1975).
- ⁵⁷Z.-Y. Ren and W. Y. Ching, *Phys. Rev. B* **23**, 5454 (1981).
- ⁵⁸G. G. De Leo, W. B. Fowler, and G. D. Watkins, *Phys. Rev. B* **29**, 3193 (1984).
- ⁵⁹W. A. Harrison, *Phys. Rev. B* **8**, 4487 (1973).
- ⁶⁰I. Honma, K. Kawai, H. Komiyama, and K. Tanaka, *Appl. Phys. Lett.* **50**, 276 (1987).
- ⁶¹S. S. Makler, P. M. Oliveira, and E. V. Anda, *J. Phys. C* **18**, 5721 (1985).
- ⁶²L. Ley, R. Kärcher, and R. L. Johnson, *Phys. Rev. Lett.* **53**, 710 (1984).
- ⁶³R. J. Sokel, *J. Phys. Chem. Solids* **41**, 899 (1980).
- ⁶⁴J. Robertson, *J. Phys. C* **17**, L349 (1984).